Simplified complex-valued modal model for operating wind turbines through aerodynamic decoupling and multi-blade coordinate transformation

Chao Chen , Philippe Duffour , Paul Fromme , Xiujiang Shen , Xugang Hua , Zhengqing Chen

PII: S0022-460X(22)00695-2
DOI: https://doi.org/10.1016/j.jsv.2022.117512
Reference: YJSVI 117512

To appear in: *Journal of Sound and Vibration*

Received date: 26 June 2022
Revised date: 8 November 2022
Accepted date: 11 December 2022

Please cite this article as: Chao Chen , Philippe Duffour , Paul Fromme , Xiujiang Shen , Xugang Hua , Zhengqing Chen , Simplified complex-valued modal model for operating wind turbines through aerodynamic decoupling and multi-blade coordinate transformation, *Journal of Sound and Vibration* (2022), doi: https://doi.org/10.1016/j.jsv.2022.117512

Highlights:

- Time-invariant state space model of wind turbine allows modal analysis in operation
- Model combining aerodynamic decoupling and multi-blade coordinate transformation
- Complex-valued modal model shows modal coupling and influence of mean wind speed
- Tower and blade dynamic responses match fully coupled model in time and frequency domain
- Modal reduction significantly reduces computation cost, allowing fast fatigue analysis

Simplified complex-valued modal model for operating wind turbines through aerodynamic decoupling and multi-blade coordinate transformation

Chao Chen[1,2], Philippe Duffour[3], Paul Fromme[4], Xiujiang Shen[1,2], and Xugang Hua[1,2*], Zhengqing Chen[1,2]

[1]Key Laboratory for Wind and Bridge Engineering, Hunan University, Changsha, China

[2]College of Civil Engineering, Hunan University, Changsha, China

[3]Department of Civil, Environmental and Geomatic Engineering, University College London, United Kingdom

[4]Department of Mechanical Engineering, University College London, United Kingdom

*Corresponding author: cexghua@hnu.edu.cn

Simplified complex-valued modal model for operating wind turbines through aerodynamic decoupling and multi-blade coordinate transformation

Abstract

An efficient modelling methodology for steady-state operating wind turbines is proposed, combining aerodynamic decoupling, multi-blade coordinate transformation, and modal reduction. This leads to a complex-valued, reduced-order modal model for prediction of dynamic responses of the tower-rotor-blade wind turbine system, considering rotor rotation, blade flexibility, and vibration coupling between rotor and tower. A fully coupled finite element model was first developed, with aerodynamic forces linearised and expressed as a viscous aerodynamic damping matrix. A time-invariant state space model is formed using multi-blade coordinate transformation, allowing standard modal analysis. The complex-valued eigenvalues and mode shapes were obtained, and it is shown that the operating wind turbine modes exhibit a combination of tower and blade vibrations. Various degrees of modal reduction are applied to the state space model to obtain a modal model with fewer degrees of freedom, whose performance was evaluated in the time and frequency domain for operating wind turbines in normal condition. The displacement and stress responses are in close agreement with those of the fully coupled model with the first 21 modes included. The model already performs well with 8 modes considered to capture relevant fundamental frequency peaks. This allows significantly reduced computational effort and can be particularly beneficial for fatigue prediction, reliability analysis, and structural identification.

Keywords: Wind turbines; aerodynamic damping; multi-blade coordinate transformation; complex modal analysis.

1 Introduction

Wind turbine modelling is usually based on multibody dynamics, in which the motions of rigid bodies (e.g., nacelle, hub) and flexible bodies (e.g., tower, blades) are coupled at every time step. Given the instantaneous blade vibration velocities, the aerodynamic loading on the rotor is calculated at every time step using the unsteady blade element momentum (BEM) theory [1]. Fully coupled models have been developed using multi-body-dynamics-based modelling techniques in wind turbine modelling packages such as FAST [2] and HAWC2 [3]. This modelling approach is beneficial to take into account the complex interaction between different components, the wind-structure interaction, and the influence of the control system. However, such fully coupled models are usually numerically demanding and thus require significant computation time which may be excessive for fatigue or reliability analyses where a large number of simulations are required. In order to obtain exact dynamic responses, more complex finite element analyses for wind turbines can be employed [4, 5].

Simplified wind turbine models have been developed (e.g., [6–8]) to improve computational speed. In these studies, aerodynamic decoupling between tower and rotor is used to simplify wind turbine models. It is usually implemented by applying the resultant rotor thrust at the tower top as a point load, with aerodynamic damping ratios representing the aerodynamic damping, and the rotor-nacelle assembly (RNA) mass lumped at the tower top ([6, 8]). However, aerodynamic damping ratios cannot accurately capture the complex aerodynamic wind-rotor interaction. Chen et al. ([9, 10]) developed an aerodynamic damping matrix to model the aerodynamic damping coupling between the fore-aft (FA) and side-side (SS) directions to better capture the wind-rotor interaction, considering the influence of tower motions. The blades were assumed to be rigid, so the blade vibration was not included, and the aerodynamic damping matrix describes the overall aerodynamic damping caused by the wind-rotor interaction to the tower, but not the aerodynamic damping of individual blades. To quantify the aerodynamic damping associated with blade bending, studies focussed on linearising the aerodynamic forces in the blade sections. For example, Rasmussen et al. [11] and Petersen et al. [12] presented the linearisation of aerodynamic forces applied to blade elements, in which the blade aerodynamic damping is represented by a 2 by 2 aerodynamic damping matrix. Linearisation is also employed in FAST [13] by combining all

linearised matrices together to form the full-system linear state-space model at an operating point. Wind turbine models have also been linearised in the frequency domain [14].

For fully coupled models, system matrices are usually time-varying for operating wind turbines due to the rotor rotation [15]. This prevents the use of conventional modal analysis of the wind turbine dynamic system. Modal analysis can be a powerful tool to simplify dynamic systems, as it allows the behaviour of systems with a large number of degrees of freedom to be captured by a limited number of dominant modes. Conducting a modal analysis on an operating wind turbine first requires converting the wind turbine system into a time-invariant one. Different methods are available to do this, such as multi-blade coordinate (MBC) transformation [16] (or Coleman transformation) and Lyapunov–Floquet (L-F) transformation [17]. Skjoldan and Hansen [17] showed that MBC transformation is a special case of L-F transformation, and that L-F transformation introduces an indeterminacy on the system frequencies. Hansen [18] stated that MBC transformation is a more physically consistent way to set up an eigenvalue problem for operating wind turbines compared to Floquet theory. MBC transformation has been used for modal analysis and modal identification of wind turbines. For example, Hansen ([18–20]) implemented MBC transformation and modal analysis to study the stall-induced edgewise blade vibrations and aeroelastic stability of wind turbines. Skjoldan and Hansen [21] investigated the effect of wind shear on modal damping based on a linearised model of a wind turbine and MBC transformation.

Operational modal analysis (OMA) is often used to identify the modal parameters of the system such as natural frequencies, modal damping ratios, and mode shapes from dynamic responses caused by ambient loads. This is partially due to a smaller number of parameters needed to be identified for a modal model. A time-varying system needs to be converted into a time-invariant one so that traditional OMA methods can be used. Alternatively, specific identification techniques need to be implemented to identify time-varying systems. For instance, Allen et al. [22] developed an output-only identification method based on the harmonic transfer function concept to identify modal parameters of a linear time-periodic wind turbine model. Yang, Tcherniak, and Allen [23] compared two modal identification methods applicable to operating wind turbines. The

first method used a conventional modal analysis (stochastic subspace identification algorithm) to identify the modal parameters after an MBC transformation. The second method utilised the harmonic power spectrum to identify a periodic model for the wind turbine.

Although aerodynamic decoupling and MBC transformation have been implemented to develop simplified wind turbine models and form the basis of wind turbine system identification, combining advanced aerodynamic decoupling, MBC transformation, and modal reduction has not been investigated for dynamic response calculation of wind turbines. This paper shows that combining the above techniques results in a complex-valued modal model (CMM) that has a significantly reduced number of degrees of freedom (DOFs) and can capture the main low-order dynamic characteristics of wind turbines. Thus, the CMM developed here provides some insight into the underlying dynamic features of the wind turbine system. As the number of DOFs considered can be significantly reduced compared to a fully coupled Finite Element (FE) model, the computational effort needed for this model is much lower. This paper is organised as follows. Section 2 describes the fully coupled model used as reference. Section 3 proposes the methodology to derive the CMM from the fully coupled model. Section 4 shows the modal analysis results and section 5 presents dynamic response analysis. Conclusions are provided in Section 6.

2 Reference model and load description

2.1 *Fully coupled aeroelastic reference model*

In the present study, a fully coupled aeroelastic model of an onshore wind turbine, including a flexible tower supporting a rotor with flexible blades, was implemented in Matlab as a reference model [24]. The schematic of this model is shown in Fig. 1(a). The derivation of the reduced CMM presented subsequently is based on this model. As this study concentrates on the wind-rotor-tower interaction, the wind turbine demonstrated in this study is onshore and only contains a rotor with three blades, a nacelle and a tower fixed at the bottom. Soil-structure interaction (SSI) is not considered in the present model for simplicity. Simplified SSI can be included by introducing linear soil springs and dashpots at the tower bottom [24]. However, the nonlinearity introduced by SSI cannot be considered in the development of the linear CMM. The fully coupled

model is a three-dimensional FE model and the aerodynamic forces are computed using unsteady BEM theory. The wind turbine model is based on the widely used 5MW reference onshore wind turbine published by NREL [25]. The basic properties of this wind turbine are listed in Table 1.

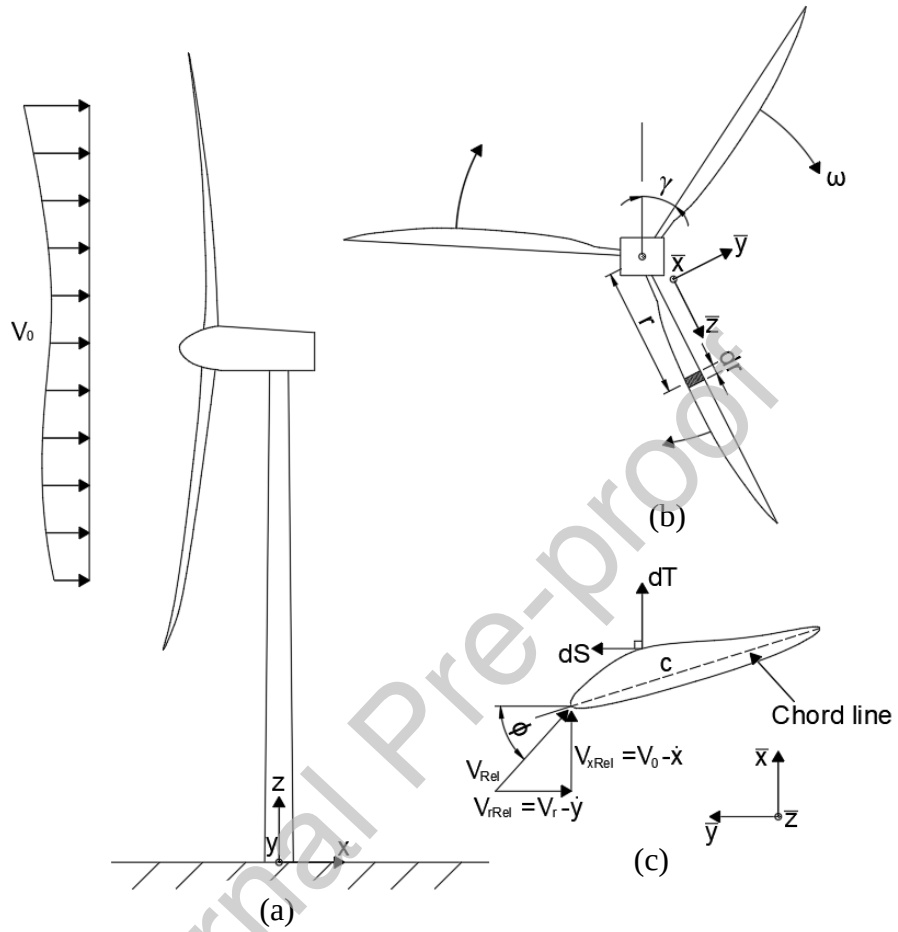

Fig. 1. Schematic of wind turbine. Side view of the system (a), front view of the rotor (b), and blade cross-section at radius r showing elemental aerodynamic forces.

Table 1 Properties of the NREL 5MW reference onshore wind turbine, based on [25].

Rotor Diameter, R	126 m
Hub Height	87.6 m
Tower Diameter, D	3.87-6.00 m
Tower Thickness, t	19-27 mm
Lumped Nacelle and Hub Mass	296780 kg
Rated Wind Speed	12.1 m/s

In the FE model, the tower and blades were modelled using three-dimensional Euler-Bernoulli beam elements. The numbers of beam elements for a single blade and the tower are 17 and 11 respectively, so the total number of beam elements in the fully coupled model is 62. For each node, there are six DOFs corresponding to three translational motions and three rotational motions, resulting in 378 DOFs overall for the fully coupled model. A convergence study confirmed that the beam element number is sufficient, as the eigenfrequency of the first mode changed by less than 1% when the number of DOFs are doubled. The finite element division of the blades is also used for the aerodynamic loading calculation using BEM so the term 'element' takes both meanings throughout the paper. Given the material and geometrical properties of the beam elements, the equations of motion of the fully coupled wind turbine model can be formulated by:

$$\mathbf{M}\ddot{\mathbf{u}} + \mathbf{C}_{Stru}\dot{\mathbf{u}} + \mathbf{K}\mathbf{u} = \mathbf{F}_{Aero}, \tag{1}$$

where $\mathbf{M}$, $\mathbf{C}_{Stru}$, $\mathbf{K}$ are the mass, structural damping, and stiffness matrices respectively, $\mathbf{F}_{Aero}$ is the external force vector containing aerodynamic forces applied to the blades. $\mathbf{u}$ is the displacement vector in the following form:

$$\mathbf{u} = [\mathbf{u}_1^{Tr}, \mathbf{u}_2^{Tr}, \dots, \mathbf{u}_{Nt}^{Tr}, \mathbf{u}_1^{B1}, \mathbf{u}_2^{B1}, \dots, \mathbf{u}_{Nb}^{B1}, \dots, \mathbf{u}_1^{B2}, \dots \mathbf{u}_{Nb}^{B2}, \mathbf{u}_1^{B3}, \dots, \mathbf{u}_{Nb}^{B3}\ ]^{\mathrm{T}}, \tag{2}$$

where Nt and Nb are the node numbers of the tower and a single blade, $\mathbf{u}_{\mathrm{i}}^{Tr}$ contains the three translational displacements and three rotations of the i^{th} tower node and $\mathbf{u}_{\mathrm{i}}^{B\mathrm{j}}$ is a vector collecting the DOFs associated with the i^{th} node in the Bj^{th} blade. $[\ ]^{\mathrm{T}}$ denotes the transpose of a matrix/vector.

In this model, the tower DOFs are referenced to a fixed inertial frame denoted by $[x, y, z]$, while the blade DOFs are expressed in local rotating frames with the rotor rotational speed ω denoted by $[\bar{x}, \bar{y}, \bar{z}]$ as shown in Fig. 1. The coordinate systems used in the above two frames are regarded as "physical coordinate systems". $\mathbf{M}$ and $\mathbf{K}$ are time-dependent matrices [26] when the wind turbine is operating. The structural damping is assumed to be proportional Rayleigh damping using the relationship $\mathbf{C} = \alpha\mathbf{M} + \beta\mathbf{K}$, where α and β are Rayleigh coefficients. These were determined such that the total damping ratios due to the structural damping are around 1% for the first tower FA and SS bending modes according to [27]. The structural damping of a single blade fixed at the hub was selected as 0.48%, following the default FAST setting. Note

that the structural damping matrix is also time-dependent, since mass and stiff matrices are. The nacelle was modelled using a concentrated mass at the tower top for simplicity, added to the mass matrix, assuming that the centre of gravity of the nacelle was located at the tower top and the nacelle's moments of inertia about all axes are zero. Time domain analyses were conducted by implementing the numerical integration scheme HHT-α [28], which is a generalised version of the Newmark-β method, as integrating the full model using a standard ODE solver (e.g. "ode45" in Matlab) proved too time-consuming.

2.2 *Wind loading*

The wind loading calculation in the fully coupled model is based on classic unsteady BEM theory ([1, 29]) with corrections. The iteration loop in a steady BEM code is neglected in the unsteady BEM code since the iteration is replaced by a time evolution, assuming that the time step chosen is sufficiently small. The corrections adopted in the unsteady BEM code include Prandtl and Glauert corrections [1]. To be consistent with the derivation leading to the aerodynamic damping matrix (described in Section 3), other corrections such as skew wake and dynamic wake corrections were not included in the unsteady BEM code.

A non-uniform turbulent inflow wind field was used as the input to the unsteady BEM code to calculate the aerodynamic forces acting on the blade elements. It was generated by a customised turbulent wind field generator coded in Matlab, producing similar wind time series compared to the wind field generator in FAST, TurbSim [30]. Kaimal spectrum was used to generate the turbulent wind field, and its relevant parameters (e.g., coherence length parameters) were selected as recommended by IEC 61400-3 [31]. The relationship between turbulence intensities and mean wind speeds at hub height was defined according to the normal turbulence model (NTM). Medium turbulence intensity (Category B) was assumed. The inflow wind velocities, the velocity caused by rotor rotation and the velocities caused by blade vibration were used as input to the unsteady BEM code. The unsteady BEM code calculates the instantaneous local aerodynamic forces for all blade elements at every time step in the time integration.

2.3 *Fully coupled model verification*

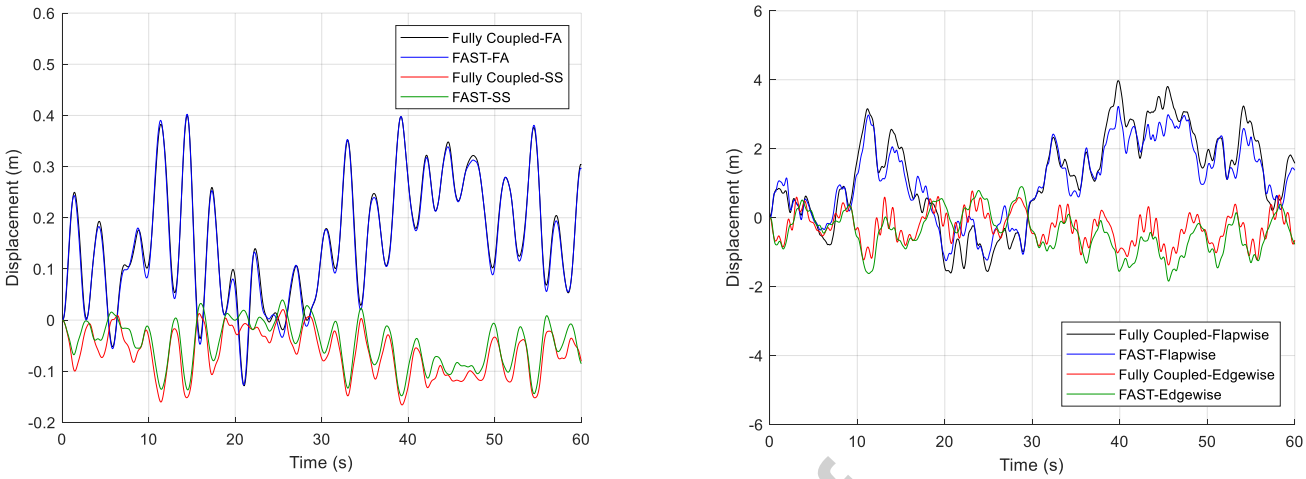

(a) (b)

Fig. 2. Tower top (a) and blade tip (b) displacement responses from the fully coupled reference model and the FAST model for a mean wind speed of 20 m/s.

FAST (version 8.15) [2] was used to verify the fully coupled reference model developed above. The NREL 5MW reference onshore wind turbine was modelled in FAST with necessary modifications (including position of nacelle and tower mode shapes) so that the FAST model is comparable to the reference fully coupled model. The turbulent wind field with a mean wind speed of 20 m/s was generated by the customised wind field generator and then input to FAST as the external excitation. The displacement responses of the tower top and blade tip from the FAST model were compared to those obtained from the fully coupled model with the same wind field, as shown in Fig. 2. Fig. 2(a) shows that the tower top responses in the FA and SS directions from these two models agree very well. In Fig. 2(b), there are slight differences between the blade tip responses from the fully coupled model and the FAST model, especially for the edge-wise direction.

FAST uses the modal superposition method to model the blade and only considers the first blade edgewise mode and the first two blade flapwise modes, while the developed fully coupled model considers more vibration modes. This can lead to the differences in the blade tip displacement responses. To quantify the accuracy of the fully coupled model in generating dynamic responses compared to the responses from the FAST model, the time response assurance criterion (TRAC) was used [32]. TRAC can be used

to quantify the degree of correlation between the two time histories. Considering two response vectors $\mathbf{u}_1(t)$ and $\mathbf{u}_2(t)$, the TRAC is defined as

$$TRAC = \frac{[\mathbf{u}_1(t)^{\mathrm{T}}\mathbf{u}_2(t)]^2}{[\mathbf{u}_1(t)^{\mathrm{T}}\mathbf{u}_1(t)][\mathbf{u}_2(t)^{\mathrm{T}}\mathbf{u}_2(t)]}, \tag{3}$$

where $\mathbf{u}_1(t)$ and $\mathbf{u}_2(t)$ have the same duration and time step. A TRAC value close to 1 indicates the two time histories are very similar. The TRAC values for the tower top displacements in the FA and SS directions are 0.9982 and 0.9483 respectively, while the TRAC values for the blade tip responses in the flapwise and edgewise directions are 0.9678 and 0.8034 respectively. These values also indicate a good agreement between the responses from the two models and confirm that the fully coupled model can generate accurate dynamic responses compared to FAST.

3 **Methodology**

3.1 ***Aerodynamic decoupling for blade elements***

It is assumed that the rotor is facing an inflow wind represented by V_0 pointing in the positive direction of the x axis. The rotor rotates positively clockwise around the x axis at a speed ω, so a blade element at distance r along the blade length moves at a speed $V_r = \omega r$ in the rotation direction, as indicated in Fig. 1(b). The azimuthal angle $\gamma_{Bj}(t)$ indicates the azimuthal position of the j^{th} blade. The vibration of the tower and blades produces a velocity in the normal direction $\dot{x}$, and a velocity in the tangential direction $\dot{y}$ in the local coordinate system. These velocities cause small variations in the relative wind speeds experienced by blade elements, as shown in Fig. 1(c). For an arbitrary blade element, the relative wind speed experienced in the normal direction, V_{xRel}, can be written as

$$V_{xRel} = V_0 - \dot{x}; \tag{4}$$

and the relative wind speed in tangential direction, V_{rRel}, is

$$V_{rRel} = V_r - \dot{y}. \tag{5}$$

Assuming that the tower and blades are rigid, the steady-state aerodynamic forces in normal and tangential directions applied to the blade element are denoted $dT(V_0, V_r)$ and $dS(V_0, V_r)$ respectively. When the tower and blades are flexible, assuming the changes in relative wind speed experienced by every blade element are sufficiently

small [9], the aerodynamic loads considering the motions of the tower and blades can be obtained using a first order Taylor expansion of the forces around the steady-state normal and tangential wind velocities. Effectively, this linearises the aerodynamic forces in terms of velocity. The force in the normal direction is given by:

$$dT(V_{xRel}, V_{rRel}) = dT(V_0, V_r) + \frac{\partial(dT)}{\partial V_0}(-\dot{x}) + \frac{\partial(dT)}{\partial V_r}(-\dot{y}); \tag{6}$$

and the force in the tangential direction is given by:

$$dS(V_{xRel}, V_{rRel}) = -\left(dS(V_0, V_r) + \frac{\partial(dS)}{\partial V_0}(-\dot{x}) + \frac{\partial(dS)}{\partial V_r}(-\dot{y})\right). \tag{7}$$

The derivation of $\frac{\partial(dT)}{\partial V_0}$, $\frac{\partial(dT)}{\partial V_r}$, $\frac{\partial(dS)}{\partial V_0}$ and $\frac{\partial(dS)}{\partial V_r}$ is provided in Appendix A. The steady-state aerodynamic forces are collected in an elemental force vector $\mathbf{F}_m^e = [dT(V_0, V_r), -dS(V_0, V_r)]^{\mathrm{T}}$. This force vector is not dependent on wind turbine vibration but becomes time-varying when wind turbulence is considered.

From Eq. 7. the elemental aerodynamic force vector can be written as

$$\mathbf{F}_{Aero}^e = \mathbf{F}_m^e - \mathbf{C}_{Aero}^e \dot{\mathbf{u}}^e, \tag{8}$$

where $\dot{\mathbf{u}}^e$ is a velocity vector expressed by $\dot{\mathbf{u}}^e = [\dot{x}, \dot{y}]^{\mathrm{T}}$. $\mathbf{C}_{Aero}^e$ is the elemental aerodynamic damping matrix for the single blade element expressed by

$$\mathbf{C}_{Aero}^e = \begin{bmatrix} \frac{\partial(dT)}{\partial V_0} & \frac{\partial(dT)}{\partial V_r} \\ -\frac{\partial(dS)}{\partial V_0} & -\frac{\partial(dS)}{\partial V_r} \end{bmatrix}. \tag{9}$$

$\mathbf{C}_{Aero}^e$ is asymmetric. The elemental aerodynamic force can be integrated over the whole rotor to obtain the resultant external force vector $\mathbf{F}_{Aero}$ in Eq. (1). The linearisation of the elemental force allows the resultant $\mathbf{F}_{Aero}$ be written as a steady-state aerodynamic force vector $\mathbf{F}_m$ plus a global aerodynamic damping matrix $\mathbf{C}_{Aero}$ multiplied by the velocity vector, which can be written as

$$\mathbf{F}_{Aero} = \mathbf{F}_m - \mathbf{C}_{Aero}\dot{\mathbf{u}}, \tag{10}$$

where $\mathbf{F}_m$ and $\mathbf{C}_{Aero}$ collect the terms in $\mathbf{F}_m^e$ and $\mathbf{C}_{Aero}^e$ at corresponding locations. $\mathbf{F}_m$ can also be calculated using the unsteady BEM theory mentioned in Section 2.2. $\mathbf{C}_{Aero}$ is also asymmetric as it collects all elemental aerodynamic damping matrices. Substituting Eq. (10) in Eq. (1), the equation of motion of the wind turbine system can be written by

$$\mathbf{M}\ddot{\mathbf{u}} + \mathbf{C}\dot{\mathbf{u}} + \mathbf{K}\mathbf{u} = \mathbf{F}_m, \tag{11}$$

where the damping matrix $\mathbf{C}$ defined by $\mathbf{C} = \mathbf{C}_{stru} + \mathbf{C}_{Aero}$ is also asymmetric.

In this way, the fully coupled wind turbine model is aerodynamically linearised because the aerodynamic forces applied on every blade element are expressed as the sum of steady-state aerodynamic forces and the elemental viscous term equal to the aerodynamic damping matrix multiplied by the blade element velocities. It should be mentioned that for certain cases (e.g., dynamic stall) the nonlinearity of the aerodynamic forces can be important and may need to be considered [1].

3.2 *Multi-blade coordinate transformation*

The system matrices in Eq. (11) are time-varying and assumed periodic i.e., $\mathbf{M}(t) = \mathbf{M}(t+T)$, $\mathbf{C}(t) = \mathbf{C}(t+T)$ and $\mathbf{K}(t) = \mathbf{K}(t+T)$, where $T = 2\pi/\omega$ is the rotor rotation period. To perform a modal reduction, the system matrices are required to be time-invariant, which is achieved using MBC transformation [18]. The MBC transformation of the displacement vector $\mathbf{u}$ is represented by

$$\mathbf{u} = \mathbf{T}\mathbf{z}, \tag{12}$$

where

$$\mathbf{T} = \begin{bmatrix} \mathbf{I}_{6Nt} & \mathbf{0} & \mathbf{0} & \mathbf{0} \\ \mathbf{0} & \mathbf{I}_{6Nb} & \mathbf{I}_{6Nb}\cos\gamma_{B1}(t) & \mathbf{I}_{6Nb}\sin\gamma_{B1}(t) \\ \mathbf{0} & \mathbf{I}_{6Nb} & \mathbf{I}_{6Nb}\cos\gamma_{B2}(t) & \mathbf{I}_{6Nb}\sin\gamma_{B2}(t) \\ \mathbf{0} & \mathbf{I}_{6Nb} & \mathbf{I}_{6Nb}\cos\gamma_{B3}(t) & \mathbf{I}_{6Nb}\sin\gamma_{B3}(t) \end{bmatrix}. \tag{13}$$

$\mathbf{I}_{6Nt}$ represents an identity matrix whose size is $6Nt \times 6Nt$. This transformation converts the three blade displacements $\mathbf{u}_i^{B1}$, $\mathbf{u}_i^{B2}$ and $\mathbf{u}_i^{B3}$ described in the local rotating coordinate system into three displacements denoted by $\mathbf{a}_{0,i}$, $\mathbf{a}_{1,i}$ and $\mathbf{b}_{1,i}$ in the MBC coordinate system, leaving the tower displacements unchanged. $\mathbf{a}_{0,i}$, $\mathbf{a}_{1,i}$ and $\mathbf{b}_{1,i}$ describe the cumulative motions of all rotor blades (not individual blades).

For the i^{th} node in the Bj^{th} blade, the displacement vector $\mathbf{u}_i^{Bj}$ is related to the MBC displacements by

$$\mathbf{u}_i^{Bj} = \mathbf{a}_{0,i} + \mathbf{a}_{1,i}\cos\gamma_{Bj}(t) + \mathbf{b}_{1,i}\sin\gamma_{Bj}(t). \tag{14}$$

The transformed displacement vector $\mathbf{z}$ is expressed as

$$\mathbf{z} = \tag{15}$$

$[\mathbf{u}_1^{Tr}, \mathbf{u}_2^{Tr}, \dots, \mathbf{u}_{Nt}^{Tr}, \mathbf{a}_{0,1}, \mathbf{a}_{0,2}, \dots, \mathbf{a}_{0,Nb}, \mathbf{a}_{1,1}, \mathbf{a}_{1,2}, \dots, \mathbf{a}_{1,Nb}, \mathbf{b}_{1,1}, \mathbf{b}_{1,2}, \dots, \mathbf{b}_{1,Nb}\ ]^{\mathrm{T}}$.

Substitute Eq. (12) into Eq. (11) and left multiplying the equations by $\mathbf{T}^{-1}$, we obtain

$$\mathbf{M}_T\ddot{\mathbf{z}} + \mathbf{C}_T\dot{\mathbf{z}} + \mathbf{K}_T\mathbf{z} = \mathbf{F}_T, \tag{16}$$

where $\mathbf{M}_T = \mathbf{T}^{-1}\mathbf{M}\mathbf{T}$, $\mathbf{C}_T = 2\mathbf{T}^{-1}\mathbf{M}\dot{\mathbf{T}} + \mathbf{T}^{-1}\mathbf{C}\mathbf{T}$, $\mathbf{K}_T = \mathbf{T}^{-1}\mathbf{M}\ddot{\mathbf{T}} + \mathbf{T}^{-1}\mathbf{C}\dot{\mathbf{T}} + \mathbf{T}^{-1}\mathbf{K}\mathbf{T}$, $\mathbf{F}_T = \mathbf{T}^{-1}\mathbf{F}_m$. The transformed mass, damping and stiffness matrices $\mathbf{M}_T$, $\mathbf{C}_T$ and $\mathbf{K}_T$ are time-invariant. As a result, the linearised model described by Eq. (11) is transformed into a time-invariant model described by Eq. (16), allowing further modal reduction.

3.3 *State space model and modal reduction*

The system matrices in Eq. (16) are asymmetric due to the MBC transformation and the asymmetry of the aerodynamic damping matrix, but complex eigenvalue analysis can still be carried out using these matrices to obtain a CMM. It is more convenient to do this after formulating the equations in state space as described in Eq. (17):

$$\mathbf{A}\dot{\mathbf{x}} + \mathbf{B}\mathbf{x} = \mathbf{f}, \tag{17}$$

where

$$\mathbf{x} = \begin{bmatrix}\dot{\mathbf{z}}\\ \mathbf{z}\end{bmatrix},$$

$$\mathbf{A} = \begin{bmatrix}\mathbf{0} & \mathbf{M}_T\\ \mathbf{M}_T & \mathbf{C}_T\end{bmatrix},$$

$$\mathbf{B} = \begin{bmatrix}-\mathbf{M}_T & \mathbf{0}\\ \mathbf{0} & \mathbf{K}_T\end{bmatrix},$$

$$\mathbf{f} = \begin{bmatrix}\mathbf{0}\\ \mathbf{F}_T\end{bmatrix}.$$

The vibration modes of dynamic system described by Eq. (17) are complex. For the k^{th} mode, the complex eigenvalue λ_k and eigenvector (or mode shape vector) $\boldsymbol{\phi}_k$ are related to $\mathbf{A}$ and $\mathbf{B}$ by:

$$(\lambda_k\mathbf{A} + \mathbf{B})\boldsymbol{\phi}_k = 0 \tag{18}$$

where $k = 1, 2, 3, \dots, N_{dof}$, and N_{dof} is the total number of DOFs for the system described by Eq. (1). The eigenvalue λ_k can be related to a complex pair calculated from the eigenfrequency $\omega_{n,k}$ and the damping factor ζ_k by

$$\lambda_k = -\zeta_k\omega_{n,k} \pm \mathrm{i}\omega_{n,k}\sqrt{1-\zeta_k^2} \tag{19}$$

where $\mathrm{i}^2 = -1$. Let the complex mode shape matrix $\boldsymbol{\Phi}$ collect all the mode shape vectors as columns. The size of $\boldsymbol{\Phi}$ is $2N_{dof} \times 2N_{dof}$. The eigenfrequencies and mode shapes mentioned here are eigen properties of the MBC transformed system with constant coefficients, but not strictly speaking of the original time-varying system. However, in previous studies relevant to wind turbine modal dynamics, the eigenfrequencies and modes of the transformed system have been regarded as the modal properties of an operating wind turbine for simplicity [18, 33]. To be clear, the eigenfrequencies, mode shapes and damping ratios are referred to the eigen properties of the MBC transformed wind turbine system throughout this study.

Implementing the transformation defined by $\mathbf{x} = \boldsymbol{\Phi}\boldsymbol{\alpha}$ and multiplying Eq. (17) by $\boldsymbol{\Phi}^{\mathrm{H}}$, the CMM of the wind turbine system can be expressed by

$$\boldsymbol{\Phi}^{\mathrm{H}}\mathbf{A}\boldsymbol{\Phi}\dot{\boldsymbol{\alpha}} + \boldsymbol{\Phi}^{\mathrm{H}}\mathbf{B}\boldsymbol{\Phi}\boldsymbol{\alpha} = \boldsymbol{\Phi}^{\mathrm{H}}\mathbf{f}, \tag{20}$$

or in a simplified form

$$\bar{\mathbf{A}}\dot{\boldsymbol{\alpha}} + \bar{\mathbf{B}}\boldsymbol{\alpha} = \bar{\mathbf{f}}, \tag{21}$$

where $\bar{\mathbf{A}} = \boldsymbol{\Phi}^{\mathrm{H}}\mathbf{A}\boldsymbol{\Phi}$, $\bar{\mathbf{B}} = \boldsymbol{\Phi}^{\mathrm{H}}\mathbf{B}\boldsymbol{\Phi}$, $\bar{\mathbf{f}} = \boldsymbol{\Phi}^{\mathrm{H}}\mathbf{f}$, $\boldsymbol{\alpha}$ is the general complex modal coordinate. $[\,]^{\mathrm{H}}$ denotes the complex conjugate (Hermitian) transpose of a matrix/vector. It should be noted that the terms in $\bar{\mathbf{A}}$, $\bar{\mathbf{B}}$ and $\bar{\mathbf{f}}$ are in general complex. The CMM is time-invariant and includes the aerodynamic damping effect explicitly. As $\mathbf{C}$ in Eq. (11) is asymmetric, $\mathbf{C}_T$ and A are both asymmetric. As a result, the equations of motion in Eq. (17) cannot in general be transformed into a system of uncoupled equations because the off-diagonal terms in $\bar{\mathbf{A}}$ and $\bar{\mathbf{B}}$ are non-zero. These off-diagonal terms represent coupling between different modes.

Considering only a limited number of dominant modes can generate wind turbine dynamic responses with sufficient accuracy, so the number of DOFs in the simplified system is lower than that in the fully coupled model. The reduced CMM with only N_{mod} modes considered can be expressed by:

$$\bar{\mathbf{A}}_r\dot{\boldsymbol{\alpha}}_r + \bar{\mathbf{B}}_r\boldsymbol{\alpha}_r = \bar{\mathbf{f}}_r, \tag{22}$$

where $\bar{\mathbf{A}}_r$, $\bar{\mathbf{B}}_r$, $\bar{\mathbf{f}}_r$ and are obtained by truncating $\bar{\mathbf{A}}$, $\bar{\mathbf{B}}$ and $\bar{\mathbf{f}}$ considering the terms relevant to the first N_{mod} modes only. It can be shown that if there is no coupling between modes (off-diagonal terms are all zero), Eq. (22) consists of a set of uncoupled equations and the solution of each equation should be the same no matter how many

modes are considered. However, the solution of Eq. (22) depends on the number of modes considered due to the coupling between modes, and it can be implied that with the increase of modes this solution slowly converges. The wind turbine model is linearised from the fully coupled model, where nonlinear rotor aerodynamics and geometrical nonlinear effects in structural members cannot be considered. However, in this study we will show that for steady operating conditions, this linear model is able to capture the main dynamic characteristics of wind turbines and generate close dynamic responses compared to those from the fully coupled reference model.

3.4 *Modal superposition*

Simulating the dynamic responses of the wind turbine system using the simplified CMM first requires the complex-valued differential equations in Eq. (22) to be solved to obtain the truncated modal coordinate $\boldsymbol{\alpha}_r$. The Matlab routine "ode45" was used to solve the complex-valued differential equations. $\mathbf{x}$ and $\mathbf{z}$ can then be calculated using the complex modal superposition method defined by $\mathbf{x} \approx \boldsymbol{\Phi}_r \boldsymbol{\alpha}_r$. To obtain the displacement vector $\mathbf{u}$ in the physical coordinate system, the transformation denoted by $\mathbf{u} = \mathbf{T}\mathbf{z}$ is finally used. The relationship between $\mathbf{u}$ and $\boldsymbol{\alpha}$ can be written by

$$\mathbf{u} \approx \mathbf{T}\boldsymbol{\Phi}_{disp,r}\boldsymbol{\alpha}_r \tag{23}$$

where $\boldsymbol{\Phi}_{disp,r}$ is the reduced $N_{dof} \times N_{mod}$ mode shape matrix obtained by truncating $\boldsymbol{\Phi}$ to only include terms related to displacement and the first N_{mod} modes. It should be noted that $\boldsymbol{\Phi}_{disp,r}$ is the truncated mode shape matrix of the time invariant system described by Eq. (17), in which the blade motions are described in the MBC transformed coordinate system. As a result, it is difficult to represent $\boldsymbol{\Phi}_{disp,r}$ graphically. Alternatively, a periodic mode shape matrix defined by $\boldsymbol{\Psi}_r = \mathbf{T}\boldsymbol{\Phi}_{disp,r}$ can be used to illustrate the mode shapes in the physical coordinate system. Combining Eqs. (14) and (23), for the displacement vector $\mathbf{u}_i^{Bj}$ of the i^{th} node in the Bj^{th} blade, the following expression can be obtained

$$\begin{aligned}\mathbf{u}_i^{Bj} \approx & \sum_{k=1}^{N_{mod}} \boldsymbol{\phi}_{k,i,a_0}\alpha_k(t) + \sum_{k=1}^{N_{mod}} \boldsymbol{\phi}_{k,i,a_1}\cos\gamma_{Bj}(t)\,\alpha_k(t) \\ & + \sum_{j=1}^{N_{mod}} \boldsymbol{\phi}_{k,i,b_1}\sin\gamma_{Bj}(t)\,\alpha_k(t).\end{aligned} \tag{24}$$

where $\boldsymbol{\phi}_{k,i,a_0}$, $\boldsymbol{\phi}_{k,i,a_1}$ and $\boldsymbol{\phi}_{k,i,a_1}$ are the three truncated mode shape vectors related to $\mathbf{a}_{0,i}$, $\mathbf{a}_{1,i}$ and $\mathbf{b}_{1,i}$ respectively for the k^{th} mode and i^{th} node, and $\alpha_k(t)$ is the general coordinate for the k^{th} mode. This means that the blade motion can be split into three components, i.e., one symmetric component ($\mathbf{a}_{0,i}$) where all the blades deflect simultaneously, two asymmetric components ($\mathbf{a}_{1,i}$ and $\mathbf{b}_{1,i}$) where the blades deflect with a phase shift caused by changing azimuthal positions [34]. The latter two asymmetric motions are also referred as backward/forward whirling [16]. As a result, flapwise blade motions correspond to the rotor coning, tilt, and yaw respectively, while edgewise blade motions correspond to the rotor collective lag, progressive lag and regressive lag respectively ([16, 35]). From Eq. (24), it can be seen that for the k^{th} mode, $\mathbf{u}_i^{Bj}$ does not only contain the frequency components from the k^{th} eigenfrequency $\omega_{n,k}$ introduced by $\alpha_k(t)$, but also from the shifted frequencies $\omega_{n,k} - \Omega$ and $\omega_{n,k} + \Omega$ introduced by $\alpha_k(t)\cos\gamma_{Bj}(t)$ and $\alpha_k(t)\sin\gamma_{Bj}(t)$ [18]. Ω is the rotor rotational frequency and $\Omega = 1/T$. Therefore, $\mathbf{u}_i^{Bj}$ can contain many frequency components not only due to the multiples of the well-known rotor rotational frequencies (1P, 2P, 3P, …) but also the unshifted/shifted eigenfrequencies.

Following the steps described, a reduced complex modal model is obtained considering an arbitrary number of modes. To include the effect of the control system, a relationship between mean wind speed, pitch angle and rotor rotation speed [25] is used to represent the normal operational states of wind turbines, as shown in Fig. 3. This relationship is used for all cases throughout this study.

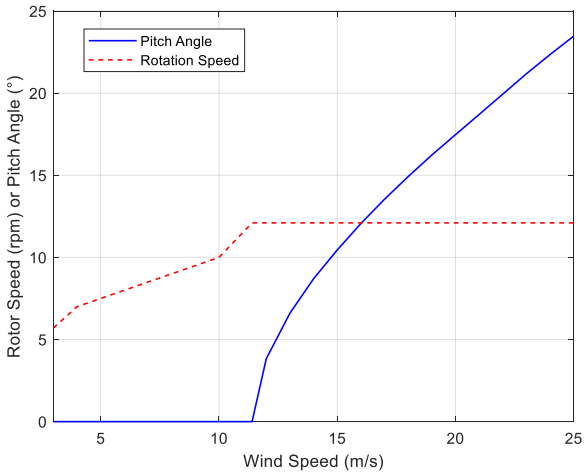

Fig. 3. Relationship between the rotor speed (dashed), pitch angle (solid) and inflow mean wind speed, based on [25].

4 **Wind turbine modal analysis**

4.1 ***Eigen properties for a single mean wind speed***

This section presents the eigen properties of the CMM developed in Section 3. The eigenfrequencies $\omega_{n,k}$ and damping factors ζ_k for the first 8 modes are listed in Table 2 for a mean wind speed of 20 m/s as an example. To obtain the vibration characteristics of a wind turbine, it is essential to include the basic vibration modes of the tower and blades, including low-order FA/SS tower vibration modes and flapwise/edgewise blade vibration modes with different vibration frequencies.The representative mode shapes (real part) of the operating wind turbine for the first 8 modes are shown in Fig. 4 in blue. Corresponding parked mode shapes are shown in red in each subplot for comparison and will be commented on later. The mode shapes shown in Fig. 4 are periodic in the original physical coordinate system. Here, one blade is always kept upward for illustration, and the fluctuation in mode shapes cannot be observed graphically.

Table 2. Eigenfrequencies, damping factors, and frequency differences for the first 8 modes; turbine parked or in operation; mean wind speed 20 m/s.

Mode Number	Operating		Parked		
	Frequency (Hz)	Damping Ratio (%)	Frequency (Hz)	Damping Ratio (%)	Frequency Difference (%)
1	0.33	1.3	0.33	1.0	2.5
2	0.35	8.6	0.34	1.0	-4.0
3	0.52	76.8	0.64	0.6	23.8
4	0.69	58.0	0.67	0.5	-3.1
5	0.84	47.8	0.70	0.5	-16.5
6	0.89	2.2	1.00	0.9	13.1
7	1.00	2.0	1.09	0.5	9.7
8	1.29	1.5	1.11	0.5	-13.7

The first mode at 0.33 Hz mainly corresponds to the first tower bending mode in the SS direction with a relatively low damping ratio of 1.3%. The second mode (0.35 Hz) can be identified as the first tower bending mode in the FA direction with a larger damping

ratio of 8.6%. This is consistent with the findings in literature that the tower is more highly damped in the FA direction when a wind turbine is in operation [27]. This mode is not a pure tower mode, as its mode shape includes significant blade flexure (combined rotor coning, tilt, and yaw). The tower also bends in the SS direction, though with much smaller amplitude. The 3rd and higher modes are dominated by rotor modes [36]. For example, the 3rd and 5th modes mainly contain rotor tilt and yaw modes, while the 4th mode is dominated by a rotor coning mode. The damping ratios for these three modes are very high (up to 76.8%), consistent with results reported in literature [33, 37] and probably due to the aerodynamic damping significantly reducing the flapwise blade vibration. On the other hand, the 6th to 8th modes are mainly rotor lag modes, with damping ratios from 1.5% to 2.2%. The 7th mode mainly corresponds to the rotor collective lag mode, while the 6th and 8th modes are dominated by rotor progressive/regressive motions. In all these modes the vibrations of the tower and three blades contribute to different extents, which makes the dynamic response of the operating wind turbine system complex.

Table 2 and Fig. 4 compare the eigenfrequencies and mode shapes of the parked wind turbine with those from the operating wind turbine, showing the influence of the aerodynamic damping on the eigen properties. The eigenfrequencies of the parked wind turbine can be regarded as the original resonance frequencies of the wind turbine system. To obtain the eigenfrequencies and mode shapes of the parked wind turbine, an eigenvalue analysis was conducted for the CMM with zero rotor rotation speed (making the MBC transformation inoperative), zero wind speed, and the initial blade positions, without aerodynamic damping. A standard eigenfrequency calculation method was used to verify this method, in which the original system matrices without aerodynamic damping were directly written in state space and then eigenfrequencies were calculated. The eigenfrequencies of the parked wind turbine calculated by these two methods are identical. As shown in Table 2, the eigenfrequencies for the first 2 modes are very similar for the parked and operating wind turbines, but significant differences can be found for other modes, especially for the 3rd and 5th modes with percentage differences larger than 15%. The differences in eigenfrequencies of the operating and parked wind turbines here are due to aerodynamics, as stiffening effects caused by rotor rotation are not considered in this study. Due to the aerodynamic damping of the operating turbine, the damping ratios of the parked wind turbine are lower, especially for the 2nd to 5th

modes. The normalized mode shapes for the parked wind turbine (red) are compared to the operating wind turbine (blue), as shown in Fig. 4. The first two mode shapes of the parked wind turbine show less combination of tower and blade vibration modes in different directions. For example, for the 1st mode, the tower only bends in the SS direction for the parked wind turbine, but the tower also bends in the FA direction for the transformed model of the operating wind turbine. In general, mode shapes of the parked and operating wind turbines are similar in terms of pattern. The mode shapes of the operating wind turbine for the rotor modes (the 3rd to 8th modes) also show some combination of flapwise and edgewise vibrations of blades. Results confirmed that the introduction of aerodynamic damping has a significant impact on all modes by increasing the coupling and motions between the different directions, so that it becomes difficult to identify the dominant mode shape component. Most higher mode shapes for the parked and operating wind turbines also follow the above trend.

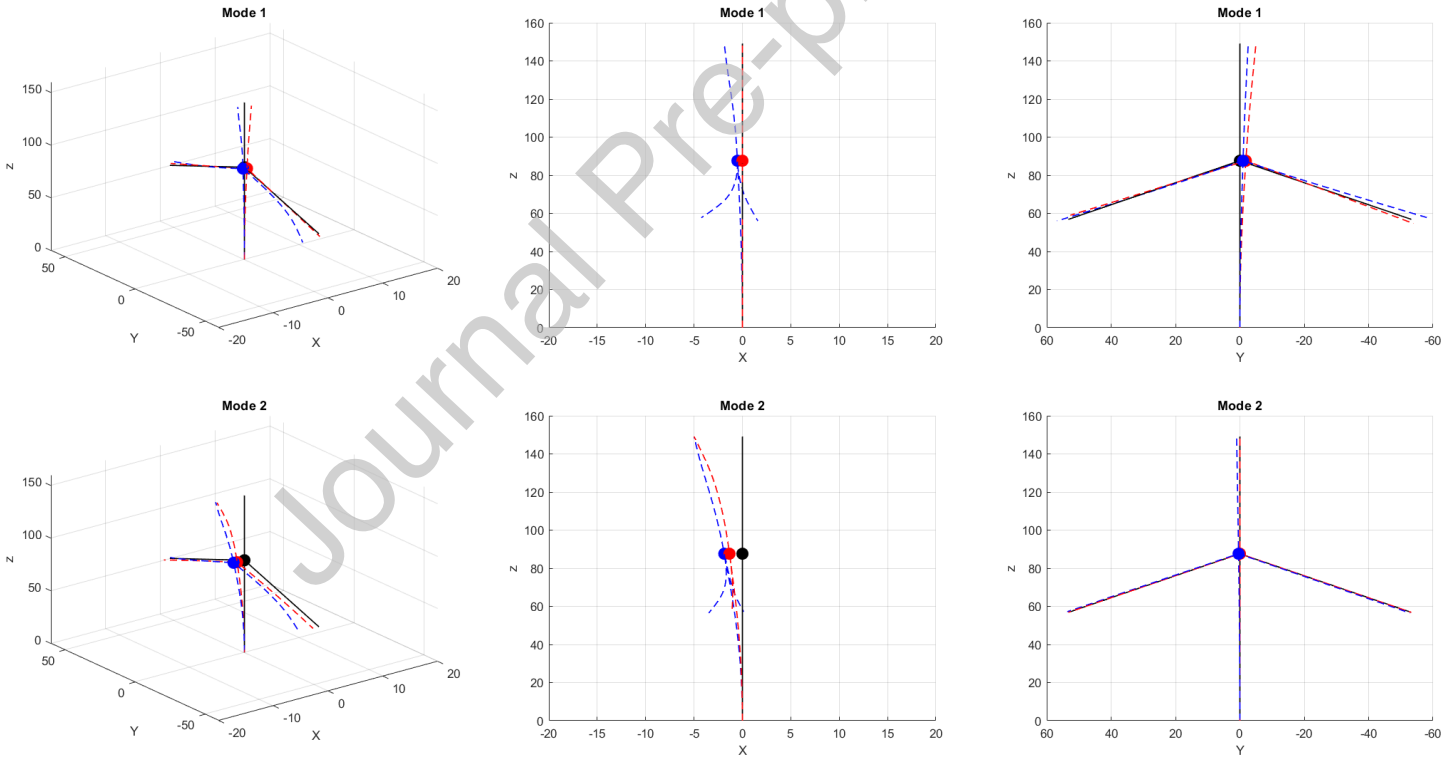

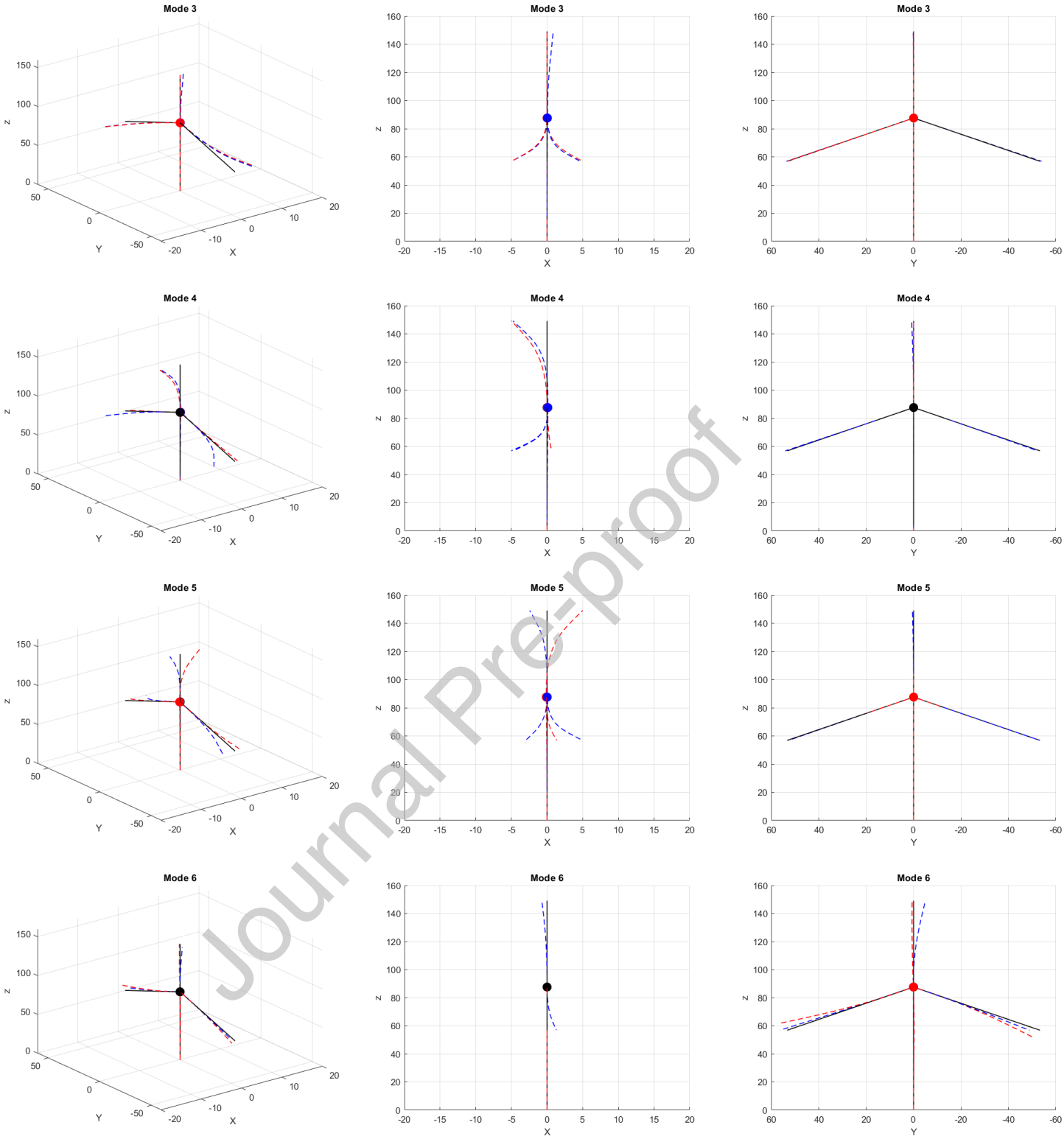

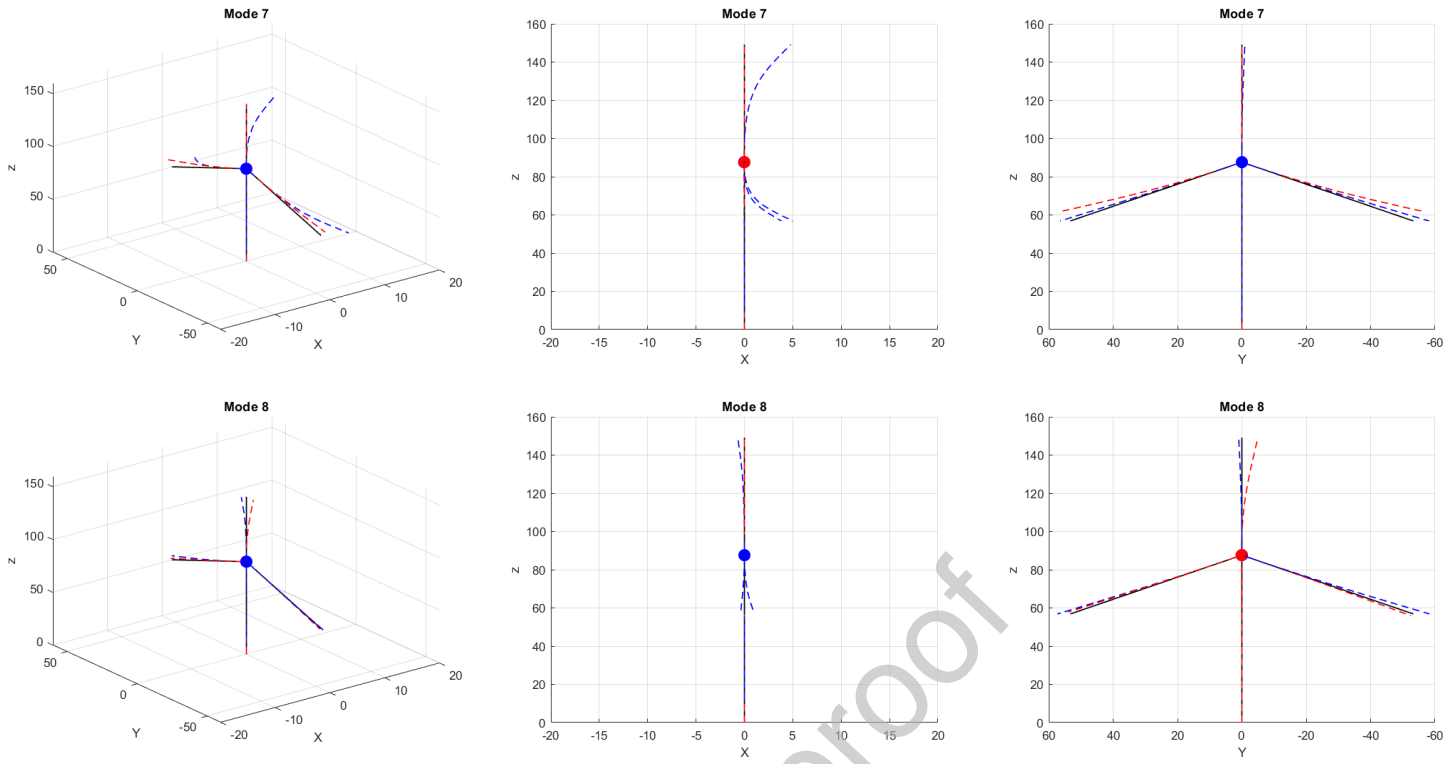

Fig. 4. Mode shapes of the first 8 modes for the operating (blue) and parked (red) wind turbines at mean wind speed 20 m/s, compared to the original position (black), with side (second column) and front views (third column).

4.2 *Influence of mean wind speed on eigen properties*

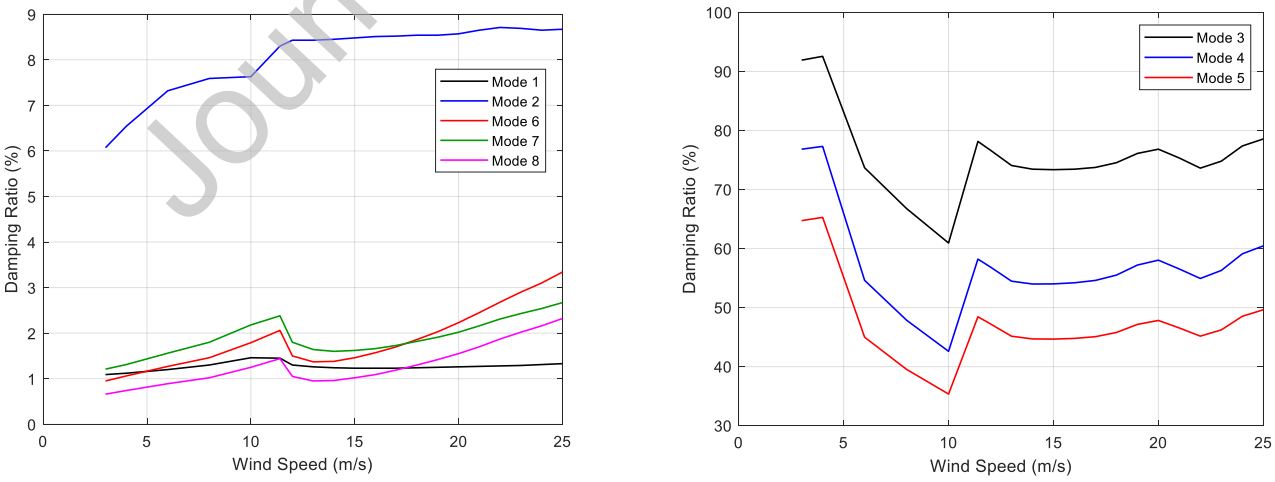

(a) (b)

Fig. 5. Damping ratios of the CMM for mean wind speeds from 3 m/s to 25 m/s.

Experimental studies have reported that the identified eigenfrequencies and damping ratios of a wind turbine system can vary with different wind speeds [38]. For the CMM, the aerodynamic damping varies with mean wind speed. Given different mean wind speeds and the corresponding rotation speeds and pitch angles (Fig. 1), the aerodynamic damping matrices were calculated, and subsequent reduced modal models were obtained. It was found that the eigenfrequencies are not significantly influenced by the mean wind speed, with an average percentage difference of 4% and a maximum percentage difference of 15% for the 3rd mode with respect to the rated wind speed (Table 2). In Fig. 5(a), the damping ratios of the CMM are plotted against the mean wind speeds for the 1st, 2nd, 6th, 7th, and 8th modes. The damping ratio for the 1st mode varies slightly between 1.1% and 1.4%. For the 2nd mode, the damping ratio increases from 6.1% to around 8.4% until the rated wind speed of 12 m/s (the blade starts to pitch) and then becomes stable around 8.5%. The relationship between the FA/SS damping ratio and mean wind speed is consistent with that reported in [9, 37, 39]. The damping ratios of the 6th to 8th modes increase from the mean wind speed of 3 m/s to the rated wind speed and then slowly increase from 14 m/s wind speed after a drop. As the damping ratios for the 3rd to 5th modes are much higher, they are shown separately in Fig. 5(b). A similar sharp drop can be observed for the damping ratios of these three modes when the mean wind speed increases from 3 m/s to 10 m/s, followed by a fluctuation of damping ratio values around 74%, 54% and 45% for the 3rd to 5th modes, respectively.

The eigenfrequencies of the operating wind turbine only vary slightly for different wind speeds or compared to the parked wind turbine. The differences in damping ratios due to the aerodynamic damping are much more noticeable, especially for the tower FA mode and flapwise rotor modes. The inclusion of aerodynamic damping causes a difference in the mode shapes for the first two modes, but much smaller mode shape differences for other modes.

5 **Dynamic response comparison**

5.1 ***Time domain simulations***

This section shows results from the time domain analysis obtained from the CMM, compared to the fully coupled model. The case with a mean wind speed of 20 m/s is again taken as an example to show the performance of the proposed model in generating

dynamic response time series, considering the first 5, 8, and 21 modes respectively. The eigenfrequencies, damping ratios for the 9th to 21st modes are shown in Appendix B, in addition to the eigen properties for the first 8 modes. The tower top responses in the FA and SS directions from the fully coupled model and the CMMs are compared in Fig. 6(a, b). Compared to the fully coupled model, 5, 8, and 21 modes capture the vibration phase and fluctuation in the tower FA displacement with good accuracy. However, for 5 and 8 modes an offset in the overall mean FA displacements can be observed. The TRAC values for the three models are 0.9877, 0.9871 and 0.9991 respectively, showing that considering the first 21 modes improves the accuracy in the tower FA response generation. For the tower SS displacement, considering either the first 8 (TRAC value: 0.9817) or 21 modes (TRAC value: 0.9888) results in close responses compared to the fully coupled model. The CMM with 5 modes is less accurate, as the blade edgewise vibrations and the tower SS vibration occur in the same plane and are closely connected.

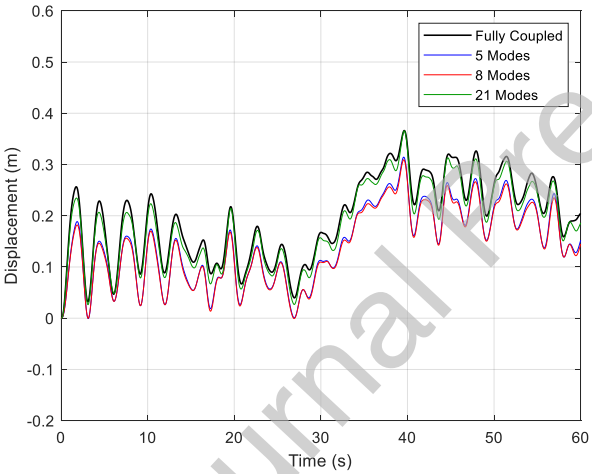

(a)

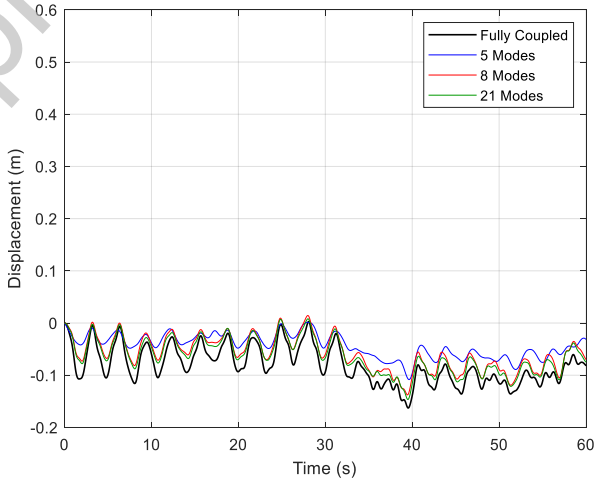

(b)

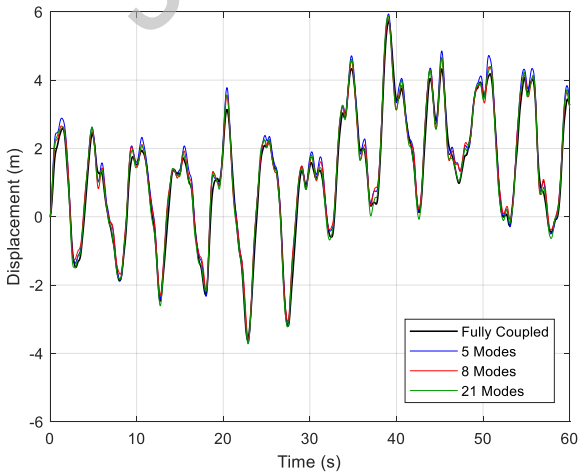

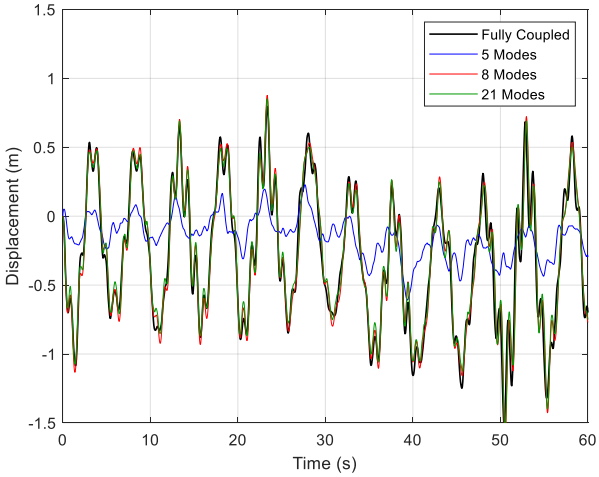

(c) (d)

Fig. 6. Tower top FA (a) and SS (b), and blade tip flapwise (c) and edgewise (d) displacement responses from the fully coupled model and the CMM including up to 21 modes for a mean wind speed of 20 m/s.

The blade tip responses of one blade from the fully coupled model and CMMs are compared in Fig. 6(c, d), showing displacements in the local rotating coordinate system of the blade. The flapwise displacements for 5, 8, and 21 modes all agree very well with those from the fully coupled model, with TRAC values around 0.9915. Differences in the edgewise responses are also small when considering enough modes, as reflected in the corresponding TRAC values of 0.9717 and 0.9737 for 8, and 21 modes, respectively. Overall, the CMM with 5 modes fails to capture the high-frequency oscillations in the edgewise blade response, as the dominant edgewise modes (6^{th} to 8^{th}) are not included. The CMMs with 8 and 21 modes successfully capture the vibration fluctuation but possibly underestimate the vibration amplitude.

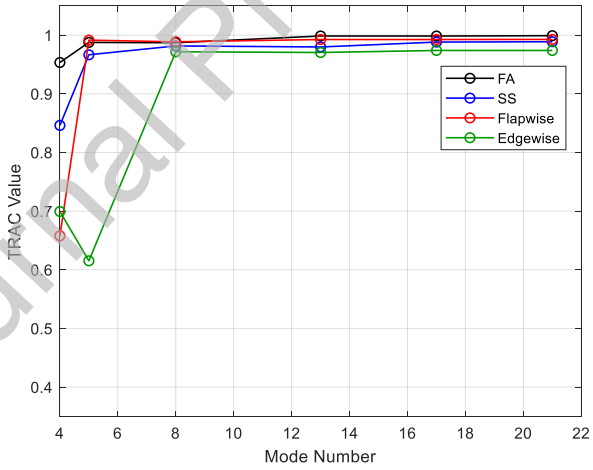

Fig. 7. TRAC values of tower FA and SS, blade tip flapwise and edgewise displacements relative to the considered mode numbers for a mean wind speed of 20 m/s.

The TRAC values for the four displacements are shown in Fig. 7, using different numbers of modes. When at least 5 modes are considered, the TRAC values for the tower FA/SS displacements and the blade tip flapwise displacement are all above 0.95, but for the blade tip flapwise displacement the TRAC value is only 0.6153. Considering more modes leads to more accurate predictions of the dynamic responses, especially

for the blade tip edgewise vibration. The TRAC value for all displacements is above 0.97 when the mode number is larger than 8. The dynamic responses from the fully coupled model were also compared to those from the full-size FE model with linearised aerodynamic damping. Almost identical differences in blade tip edgewise responses were obtained, showing that the slightly less accurate blade edgewise response is due to the linearised aerodynamic damping, which could overestimate the aerodynamic damping in blade edgewise vibration.

5.2 *Frequency domain comparison*

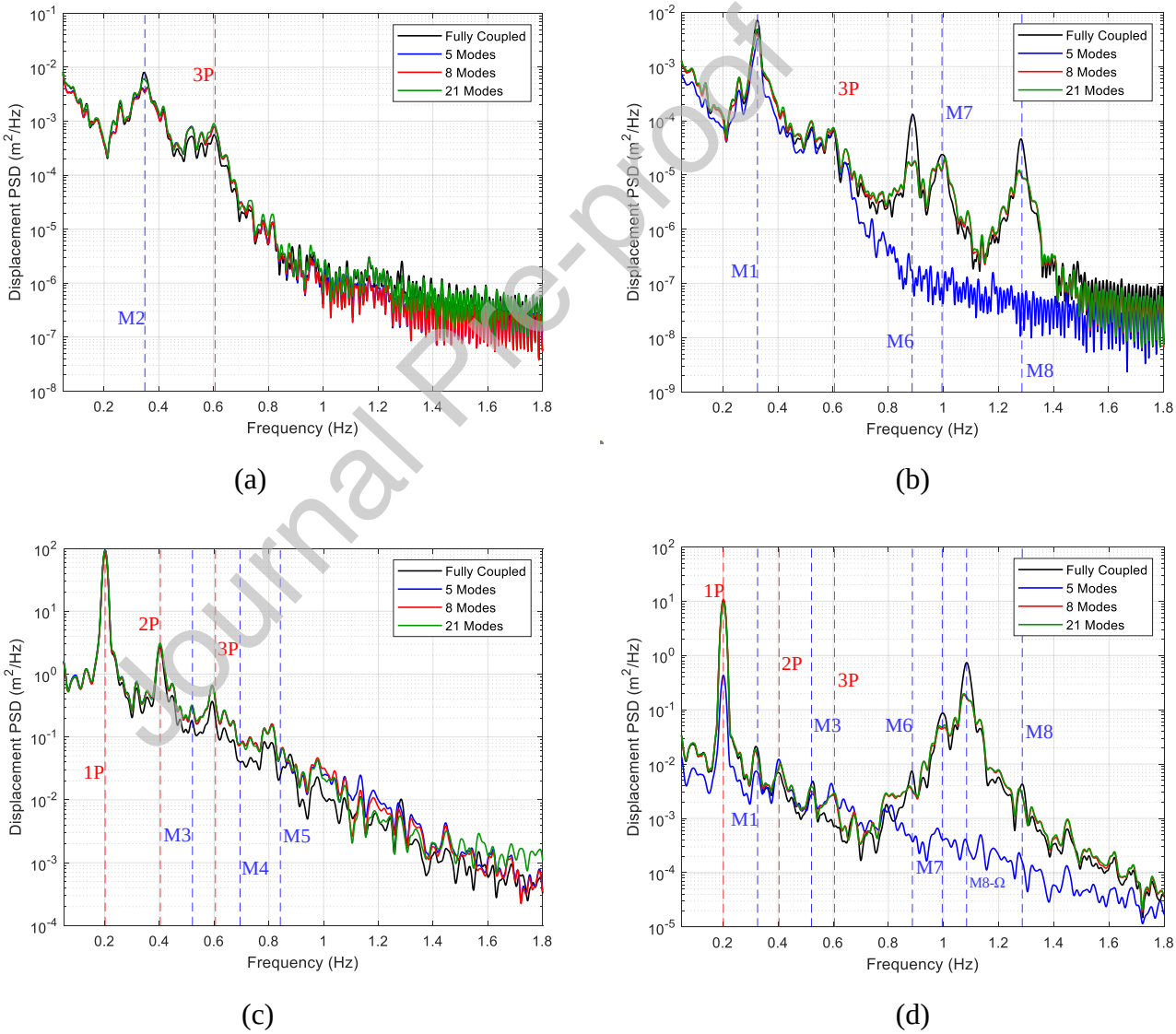

Fig. 8. Tower top FA (a) and SS (b), and blade tip flapwise (c) and edgewise (d) displacement PSDs for a mean wind speed of 20 m/s and various reduced models.

The dynamic responses generated by the CMM were also analysed in the frequency domain. The power spectral densities (PSDs) of the obtained dynamic time responses were calculated using the Matlab function "pwelch" and compared in Fig. 8 for the tower top FA and SS displacements and the blade tip flapwise and edgewise displacements. M1-8 label the frequencies of the first 8 modes, and 1P~6P represent the multiples of the rotor rotation frequency 0.2 Hz corresponding to a rotation speed of 12.1 rpm. Fig. 8(a, b) shows that the modes with frequencies close to the 1st and 2nd eigenfrequency dominate the tower top SS and FA displacement responses. In the frequency range up to 1.8 Hz, the FA tower motion for the CMMs with all levels of modal reduction results in close PSDs compared to that from the fully coupled model. However, the 5 mode model cannot capture the peaks above 0.8 Hz for the SS tower motion. In Fig. 8(b), the PSDs from the CMMs with more than 5 modes have similar peaks at eigenfrequencies for the 6th to 8th mode but with lower amplitudes compared to those from the fully coupled model. The amplitude difference could be due to the aerodynamic decoupling that overestimates the aerodynamic damping. Fig. 8(c) shows that the blade tip flapwise vibration is dominated by the peaks near 1P and 2P, which is well captured by the CMMs with 5 or more modes. The eigenfrequencies of the 3rd to 5th modes dominated by the flapwise blade vibration are between 0.5 and 0.85 Hz. The very high damping ratios of these modes can account for the fact that their peaks are not clearly visible in Fig. 8(c). The peaks near 1P and 2P are not caused by the inherent system modes, but by the harmonics in the external aerodynamic forces due to rotor rotation. Fig. 8(d) shows that the blade tip edgewise displacements are dominated by two peaks, one at the 1P frequency and one at frequency M8-Ω. The latter peak is a combination resonance between the 8th eigenfrequency and the rotor rotation which arises from product terms such as $\alpha_k(t)\sin\gamma_{Bj}(t)$ in Eq. (24). Other peaks also appear distinctly, such as peaks at the 2P frequency and the 1st eigenfrequency. Therefore, only considering the first 5 modes cannot capture the peaks above 0.8 Hz.

Time and frequency domain results are consistent, with increased accuracy of the dynamic responses when a higher number of modes is considered. Considering 8 or more modes, all relevant resonances in the frequency domain are identified, but some differences remain for the tower FA and blade edgewise displacements. Considering 21

modes (from 380 for the full model) increases the model accuracy, especially for the tower FA motion.

5.3 *Stress response prediction*

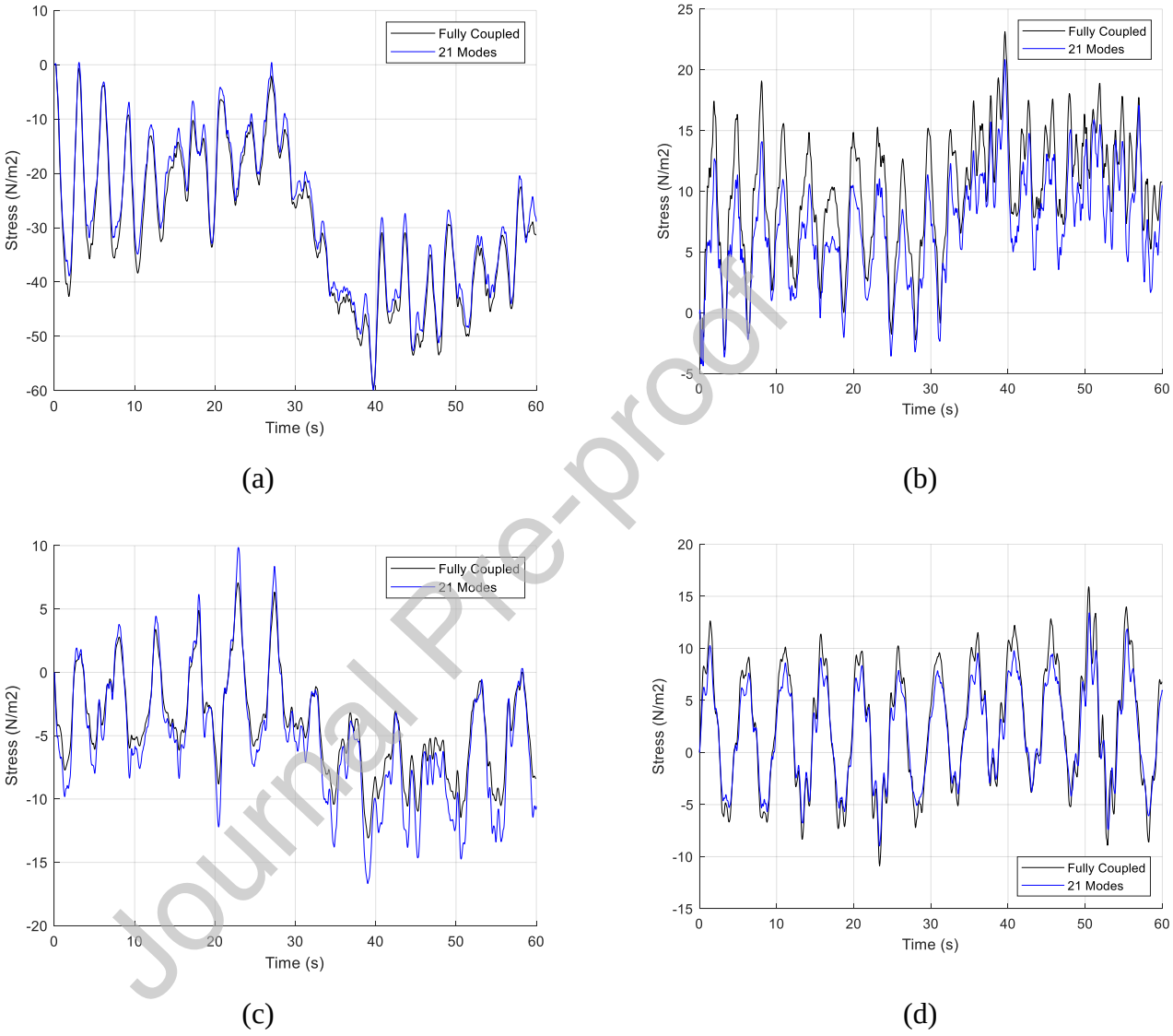

Fig. 9. Tower bottom FA (a) and SS (b), and blade root flapwise (c) and edgewise (d) longitudinal stresses from the fully coupled model and the CMM with 21 modes for a mean wind speed of 20 m/s.

One of the possible applications of the reduced CMM is to conduct efficient fatigue analyses, requiring accurate stress hotspot responses. The internal forces and stresses in the tower and blade sections can be obtained from finite element displacement output. The Euler-Bernoulli bending strains are the product of the local curvatures and the

distance from the neutral axis in each direction [24]. The curvatures can be obtained by differentiating the elemental shape functions twice. Therefore, the longitudinal stress $\sigma_{zz}(x, y, z, t)$ at time t, position $(x,\ y)$ within the cross-section and z along the tower or blade, is the linear superposition of the two strains multiplied by Young's modulus E:

$$\sigma_{zz}(x, y, z, t) = -E\left(\mathbf{N}^{e\prime\prime}(z)\mathbf{u}_x^e(t)x + \mathbf{N}^{e\prime\prime}(z)\mathbf{u}_y^e(t)y\right), \tag{25}$$

where $\mathbf{N}^{e\prime\prime}(z)$ is the second order derivative of the elemental shape function vector, $\mathbf{u}_x^e(t)$ and $\mathbf{u}_y^e(t)$ are the nodal displacement vectors in the x and y directions.

With the displacement responses generated by the CMM with 21 modes, the maximum tower bottom stresses in the FA and SS directions and blade root stresses in the flapwise and edgewise directions can be calculated using Eq. (25). The calculated stresses are found to be close to those obtained from the fully coupled model, as shown in Fig. 9, with TRAC values larger than 0.97 for all four stress time series. Although the tower bottom SS stresses are slightly underestimated using 21 modes, it can be concluded that generally accurate stress responses for the tower and blades with significantly reduced DOFs can be generated for fatigue damage analysis.

5.4 ***Computation speed comparison***

Crucially, the modal reduction results in significant computational savings, as shown in

Table 3 comparing the computation time needed for the fully coupled model in Matlab, the FAST model, and the CMM with different number of modes considered. The settings for the FAST model are as described in Section 2.3. These three models are based on different principles. The tower and blades are modelled by beam elements in the fully coupled model in Matlab, but they are modelled by modal superposition in FAST. However, the CMM is formulated by applying complex modal reduction to an aerodynamically decoupled finite element model.

Table 3. Computation time comparison for 60 s of simulation time.

	Fully coupled model	FAST model	Complex modal model		
			5 modes	8 modes	21 modes
Computation time (s)	21	10	0.07	0.07	0.63

For 60 s of simulation time, the fully coupled model requires 21 s of computation time and the FAST model takes 10 s, as the FAST model only considers two tower bending modes and two blade bending modes. However, the required computation time for the CMMs with 5 modes and 8 modes is only 0.07 s. The CMM with 21 modes is more accurate as discussed above and still requires only a very short computation time of 0.63 s for this simulation. The computation time comparison here is not like-for-like, as different integration algorithms were used. However, it can be concluded that the CMM is much more efficient than the fully coupled model and the quasi-mode based FAST model due to aerodynamic decoupling and significant reduction of DOFs. Therefore, with an appropriate number of modes considered, the CMM has the potential to conduct efficient fatigue analysis requiring large number of calculations.

6 **Conclusions**

This study proposes a novel methodology to efficiently model wind turbines by combing aerodynamic linearisation, MBC transformation, and modal reduction, resulting in a complex-valued modal model that considers the vibrations of both the tower and blades. Three steps are required to form the CMM:

1. Aerodynamic linearisation is first conducted to capture the aerodynamic forces applied to blade elements with 2×2 aerodynamic damping matrices.
2. The fully coupled model is then converted to a time-invariant state-space model using the MBC transformation.
3. Modal decomposition is implemented to obtain a reduced CMM with limited modes considered.

This model explicitly includes aerodynamic damping caused by wind-rotor interaction and considers blade flexibility. It allows standard modal analysis and investigation of the eigen properties of the system, showing that the modes of the operating wind turbine exhibit a combination of tower and blade vibration. It is found that the aerodynamic damping ratios vary with the mean wind speed and follow similar trends and amplitudes

compared to literature, while the eigenfrequencies do not change significantly with the mean wind speed.

The complex equations of motion were solved by a time integration technique and modal superposition is employed to obtain the dynamic responses of the whole wind turbine with a varying number of modes included. The dynamic responses from the CMM were compared to those from the fully coupled model in the time and frequency domains. The conclusions are:

1. Accurate dynamic time responses for displacements and hotspot stresses can be obtained when the first 21 modes are included (TRAC values above 0.97).
2. The model performs well with at least 8 modes included, in terms of effectively capturing the peaks most relevant to rotor rotation frequencies and eigenfrequencies.
3. The computation time is significantly reduced. The computation time required for the CMM with 8 modes is only around 0.3% of that for the finite-element-based fully coupled model in Matlab and 0.7% of that for the FAST model.

Hence, the CMM can be very useful when large numbers of simulations are required, such as fatigue prediction, structural optimisation, and reliability analysis. Furthermore, the model could be used as an identification target as it explicitly includes aerodynamic damping effects and has advantageous complex eigen properties that enable the overall dynamic characteristics to be captured with a limited number of modes.

Author statement

Chao Chen: Conceptualization, Methodology, Software, Writing - Original Draft, Writing - Review & Editing, Funding acquisition

Philippe Duffour: Methodology, Validation, Writing - Review & Editing

Paul Fromme: Methodology, Validation, Writing - Review & Editing

Xiujiang Shen: Data curation

Shuai Zhou: Validation

Xugang Hua: Writing - Review & Editing, Funding acquisition, Supervision

Zhengqing Chen: Supervision

7 Acknowledgement

The financial supports from the National Natural Science Foundation of China (No. 52108280) and the National Science Fund for Distinguished Young Scholars (No. 52025082) are greatly appreciated.

References

[1] Hansen MOL. *Aerodynamics of wind turbines*. 3rd ed. London, England: Routledge, 2015.

[2] Jonkman JM, Buhl ML Jr. *FAST user's guide*. Technical Report NREL/EL-500-38230. National Renewable Energy Laboratory: Golden, CO, USA, October 2005.

[3] Torben J, Melchior A. *How 2 HAWC2, the user's manual*. Technical Report Risø-R-1597(ver. 3-1)(EN). Risø National Laboratory, Denmark, 2007.

[4] Griffith DT, Ashwill TD. The Sandia 100-meter all-glass baseline wind turbine blade: SNL100-00. *Informe Técnico, Sandia National Laboratories*, https://citeseerx.ist.psu.edu/viewdoc/download?doi=10.1.1.469.653&rep=rep1&type=pdf (2011).

[5] Berg JC, Resor BR. Numerical manufacturing and design tool (NuMAD v2. 0) for wind turbine blades: user's guide, https://www.osti.gov/servlets/purl/1051715 (2012).

[6] Rezaei R, Fromme P, Duffour P. Fatigue life sensitivity of monopile-supported offshore wind turbines to damping. *Renewable Energy* 2018; 123: 450–459.

[7] Muskulus M, Schafhirt S. Reliability-based design of wind turbine support structures. In: *Proceedings of the Symposium on Reliability of Engineering System*. Hangzhou, China, 2015.

[8] Bisoi S, Haldar S. Dynamic analysis of offshore wind turbine in clay considering soil–monopile–tower interaction. *Soil Dynamics and Earthquake Engineering* 2014; 63: 19–35.

[9] Chen C, Duffour P, Fromme P. Modelling wind turbine tower-rotor interaction through an aerodynamic damping matrix. *J Sound Vib* 2020; 489: 115667.

[10] Chen C, Duffour P, Dai K, et al. Identification of aerodynamic damping matrix for operating wind turbines. *Mech Syst Signal Process* 2021; 154: 107568.

[11] Rasmussen F, Petersen JT, Madsen HA. Dynamic Stall and Aerodynamic Damping. *J Sol Energy Eng* 1999; 121: 150.

[12] Petersen JT, Madsen H a., Bjorck A, et al. *Prediction of dynamic loads and induced vibrations in stall*. Technical Report NO. 1045(EN). Forskningscenter

Risoe, Denmark, 1998.

[13] Jonkman JM, Jonkman BJ. FAST modularization framework for wind turbine simulation: Full-system linearization. *J Phys Conf Ser*; 753. Epub ahead of print 2016. DOI: 10.1088/1742-6596/753/8/082010.

[14] Lupton RC, Langley RS. Improved linearised models of wind turbine aerodynamics and control system dynamics using harmonic linearisation. *Renewable Energy* 2019; 135: 148–162.

[15] Chen B, Zhang Z, Hua X, et al. Identification of aerodynamic damping in wind turbines using time-frequency analysis. *Mech Syst Signal Process* 2017; 91: 198–214.

[16] Bir G. User ' s Guide to MBC3 : Multi-Blade Coordinate Transformation Code for 3-Bladed Wind Turbines. 2010; 32.

[17] Skjoldan PF, Hansen MH. On the similarity of the Coleman and Lyapunov-Floquet transformations for modal analysis of bladed rotor structures. *J Sound Vib* 2009; 327: 424–439.

[18] Hansen MH. Improved modal dynamics of wind turbines to avoid stall-induced vibrations. *Wind Energy* 2003; 6: 179–195.

[19] Hansen MH. Aeroelastic stability analysis of wind turbines using an eigenvalue approach. *Wind Energy* 2004; 7: 133–143.

[20] Hansen MH. Aeroelastic instability problems for wind turbines. *Wind Energy* 2007; 10: 551–577.

[21] Skjoldan PF, Hansen MH. Effects of extreme wind shear on aeroelastic modal damping of wind turbines. *Wind Energy* 2013; 16: 401–415.

[22] Allen MS, Sracic MW, Chauhan S, et al. Output-only modal analysis of linear time-periodic systems with application to wind turbine simulation data. *Mech Syst Signal Process* 2011; 25: 1174–1191.

[23] Yang S, Tcherniak D, Allen MS. Modal analysis of rotating wind turbine using multiblade coordinate transformation and harmonic power spectrum. *Conference Proceedings of the Society for Experimental Mechanics Series* 2014; 7: 77–92.

[24] Chen C, Duffour P, Fromme P, et al. Numerically efficient fatigue life prediction of offshore wind turbines using aerodynamic decoupling. *Renewable Energy* 2021; 178: 1421–1434.

[25] Jonkman JM, Butterfield S, Musial W, et al. Definition of a 5-MW reference wind turbine for offshore system development. 2009; 1–75.

[26] Staino A, Basu B. Dynamics and control of vibrations in wind turbines with variable rotor speed. *Eng Struct* 2013; 56: 58–67.

[27] Chen C, Duffour P. Modelling damping sources in monopile-supported offshore

wind turbines. *Wind Energy* 2018; 21: 1121–1140.

[28] Gavin HP. *Numerical integration in structural dynamics*. Duke University, http://people.duke.edu/~hpgavin/cee541/NumericalIntegration.pdf (2016).

[29] Branlard E. Chapter 10 The Blade ElementMomentum (BEM) Method. In: *Wind Turbine Aerodynamics and Vorticity-Based Methods*. Epub ahead of print 2017. DOI: 10.1007/978-3-319-55164-7.

[30] Jonkman BJ, Kilcher L. *TurbSim user's guide : version 1. 06.00*. Technical Report. National Renewable Energy Laboratory: Golden, CO, USA: National Renewable Energy Laboratory, 2012.

[31] International Electrotechnical Commission (IEC). IEC 61400-3 Wind turbines - Part 3: Design requirements for offshore wind turbines.

[32] Avitabile P, Pingle P. Prediction of full field dynamic strain from limited sets of measured data. *Shock Vibr Dig* 2012; 19: 765–785.

[33] Filsoof OT, Yde A, Bøttcher P, et al. On critical aeroelastic modes of a tri-rotor wind turbine. *Int J Mech Sci* 2021; 204: 106525.

[34] Heinz JC, Sørensen NN, Zahle F, et al. Vortex-induced vibrations on a modern wind turbine blade. *Wind Energy* 2016; 19: 2041–2051.

[35] Bir G, Wright AD, Butterfield CP. *Stability analysis of a variable-speed wind turbines*. 1996.

[36] Chauhan S, Tcherniak D, Basurko J, et al. Operational Modal Analysis of Operating Wind Turbines: Application to Measured Data. In: *Rotating Machinery, Structural Health Monitoring, Shock and Vibration*. Springer, New York, NY., pp. 65–81.

[37] Buhl T, Markou H, Hansen MH, et al. Aeroelastic stability analysis and passive instability suppression. *European Wind Energy Conference and Exhibition 2006, EWEC 2006* 2006; 2: 1666–1676.

[38] Dong X, Lian J, Wang H, et al. Structural vibration monitoring and operational modal analysis of offshore wind turbine structure. *Ocean Eng* 2018; 150: 280–297.

[39] Valamanesh V, Myers AT. Aerodynamic Damping and Seismic Response of Horizontal Axis Wind Turbine Towers. *J Struct Eng* 2014; 140: 1–9.

Appendix A

Derivation for partial derivatives used in Section 3

This appendix gives the expressions necessary to calculate the partial derivatives defining the aerodynamic damping matrix in terms of known aerodynamic quantities such as inflow wind speed, blade profile, fluid properties and operational conditions. All notations used here are from the classic steady BEM theory [1]. These partial derivatives are $\frac{\partial(dT)}{\partial V_x}$, $\frac{\partial(dT)}{\partial V_r}$, $\frac{\partial(dS)}{\partial V_x}$ and $\frac{\partial(dS)}{\partial V_r}$. The derivation based on the variables V_0 and V_r is given. According to BEM theory, the thrust on an element at radius r can be written as

$$dT = \frac{1}{2}\rho[V_0^2(1-a)^2 + V_r^2(1+a')^2]C_n c dr, \quad \text{(A. 1)}$$

where ρ is the air density, a and a' are the axial and tangential induction factors respectively, c is the chord length, C_n is the normal force coefficient and dr is the increment length of the element. The tangential force can be expressed by

$$dS = \frac{1}{2}\rho[V_0^2(1-a)^2 + V_r^2(1+a')^2]C_t c dr, \quad \text{(A. 2)}$$

where C_t is the tangential force coefficient. Assuming dT and dS are functions of V_0 and V_r, other intermediate variables such as a, a', C_n, C_t and ϕ can also be treated as functions with regard to V_0 and V_r. ϕ is the sum of the attack angle, pitch and twist angles. According to classic BEM theory, the relationships between these variables are

$$a = \frac{1}{\frac{4\,sin^2\phi}{\sigma C_n} + 1}, \quad \text{(A. 3)}$$

where σ indicates the solidity,

$$a' = \frac{1}{\frac{4sin\phi cos\phi}{\sigma C_t} - 1}; \quad \text{(A. 4)}$$

and

$$C_n = C_l cos\phi + C_d sin\phi, \quad \text{(A. 5)}$$

and

$$C_t = C_l sin\phi - C_d cos\phi; \quad \text{(A. 6)}$$

where C_l and C_d is the lift and drag coefficients respectively,

and

$$tan\phi = \frac{V_0(1-a)}{V_r(1+a')} \; or \; cot\phi = \frac{V_r(1+a')}{V_0(1-a)}. \qquad (A.\ 7)$$

Firstly, from Equation (A. 1), $\frac{\partial(dT)}{\partial V_0}$ can be written as

$$\frac{\partial(dT)}{\partial V_0} = \frac{1}{2}\rho c \cdot dr \cdot \left[\frac{\partial(V_{Rel}^2)}{\partial V_0} C_n + V_{Rel}^2 \frac{\partial C_n}{\partial V_0}\right], \qquad (A.\ 8)$$

where $V_{Rel}^2 = V_0^2(1-a)^2 + V_r^2(1+a')^2$;

$\frac{\partial(dT)}{\partial V_r}$ can be written as

$$\frac{\partial(dT)}{\partial V_r} = \frac{1}{2}\rho c \cdot dr \cdot \left[\frac{\partial(V_{Rel}^2)}{\partial V_r} C_n + V_{Rel}^2 \frac{\partial C_n}{\partial V_r}\right]. \qquad (A.\ 9)$$

Similarly, from Equation (A. 2),

$$\frac{\partial(dS)}{\partial V_0} = \frac{1}{2}\rho c \cdot dr \cdot \left[\frac{\partial(V_{Rel}^2)}{\partial V_0} C_t + V_{Rel}^2 \frac{\partial C_t}{\partial V_0}\right]; \qquad (A.\ 10)$$

and

$$\frac{\partial(dS)}{\partial V_r} = \frac{1}{2}\rho c \cdot dr \cdot \left[\frac{\partial(V_{Rel}^2)}{\partial V_r} C_t + V_{Rel}^2 \frac{\partial C_t}{\partial V_r}\right]. \qquad (A.\ 11)$$

The expression for the terms in Equations (A. 8) to (A. 11) can be expressed as follows:

$$\frac{\partial(V_{Rel}^2)}{\partial V_0} = 2V_0(1-a)^2 - V_0^2 \cdot 2(1-a)\frac{\partial a}{\partial V_0} + V_r^2 \cdot 2(1+a')\frac{\partial a'}{\partial V_0} \qquad (A.\ 12)$$

where $\frac{\partial a}{\partial V_0} = \frac{da}{d\phi} \cdot \frac{\partial \phi}{\partial V_0}$ and $\frac{\partial a'}{\partial V_0} = \frac{da'}{d\phi} \cdot \frac{\partial \phi}{\partial V_0}$;

Then

$$\frac{\partial(V_{Rel}^2)}{\partial V_r} = -V_0^2 \cdot 2(1-a)\frac{\partial a}{\partial V_r} + 2V_r(1+a')^2 + V_r^2 \cdot 2(1+a')\frac{\partial a'}{\partial V_r} \qquad (A.\ 13)$$

where $\frac{\partial a}{\partial V_r} = \frac{da}{d\phi} \cdot \frac{\partial \phi}{\partial V_r}$ and $\frac{\partial a'}{\partial V_r} = \frac{da'}{d\phi} \cdot \frac{\partial \phi}{\partial V_r}$.

$\frac{da}{d\phi}$ and $\frac{da'}{d\phi}$ can be determined from Equations (A. 3) and (A. 4):

$$\frac{da}{d\phi} = \frac{-4\left(sin2\phi C_n - \frac{dC_n}{d\phi} sin^2\phi\right)}{\sigma C_n^2 \left(\frac{4sin^2\phi}{\sigma C_n} + 1\right)^2}, \qquad (A.\ 14)$$

and

$$\frac{da'}{d\phi} = \frac{-4\left(cos2\phi C_t - \frac{dC_t}{d\phi} sin\phi cos\phi\right)}{\sigma C_t^2 \left(\frac{4sin\phi cos\phi}{\sigma C_t} - 1\right)^2}. \qquad (A.\ 15)$$

The expressions for $\frac{\partial\phi}{\partial V_0}$ and $\frac{\partial\phi}{\partial V_r}$ can be found from Equation (A. 7) using the following two equations:

$$\frac{\partial\phi}{\partial V_0}\left[\frac{d\left(\frac{1+a'}{1-a}\right)}{d\phi}tan\phi+\frac{1}{cos^2\phi}\cdot\frac{1+a'}{1-a}\right]=\frac{1}{V_r} \quad (A.\ 16)$$

and

$$\frac{\partial\phi}{\partial V_r}\left[\frac{d\left(\frac{1-a}{1+a'}\right)}{d\phi}cot\phi-\frac{1}{sin^2\phi}\cdot\frac{1-a}{1+a'}\right]=\frac{1}{V_0}. \quad (A.\ 17)$$

where $\frac{d\left(\frac{1+a'}{1-a}\right)}{d\phi}=\frac{\frac{da'}{d\phi}(1-a)+\frac{da}{d\phi}(1+a')}{(1-a)^2}$ and $\frac{d\left(\frac{1-a}{1+a'}\right)}{d\phi}=\frac{-\frac{da}{d\phi}(1+a')-\frac{da'}{d\phi}(1-a)}{(1+a')^2}$.

For $\frac{\partial C_n}{\partial V_0}$, $\frac{\partial C_n}{\partial V_r}$, $\frac{\partial C_t}{\partial V_0}$ and $\frac{\partial C_t}{\partial V_r}$, the following four equations can be used:

$$\frac{\partial C_n}{\partial V_0}=\frac{dC_n}{d\phi}\cdot\frac{\partial\phi}{\partial V_0}; \quad (A.\ 18)$$

$$\frac{\partial C_n}{\partial V_r}=\frac{dC_n}{d\phi}\cdot\frac{\partial\phi}{\partial V_r}; \quad (A.\ 19)$$

$$\frac{\partial C_t}{\partial V_0}=\frac{dC_t}{d\phi}\cdot\frac{\partial\phi}{\partial V_0}; \quad (A.\ 20)$$

$$\frac{\partial C_t}{\partial V_r}=\frac{dC_t}{d\phi}\cdot\frac{\partial\phi}{\partial V_r}. \quad (A.\ 21)$$

$\frac{dC_n}{d\phi}$ and $\frac{dC_t}{d\phi}$ can be simply derived from Equations(A. 5) and (A. 6):

$$\frac{dC_n}{d\phi}=\frac{\partial C_l}{\partial\phi}cos\phi+\frac{\partial C_d}{\partial\phi}sin\phi+C_d cos\phi-C_l sin\phi, \quad (A.\ 22)$$

and

$$\frac{dC_t}{d\phi}=\frac{\partial C_l}{\partial\phi}sin\phi-\frac{\partial C_d}{\partial\phi}cos\phi+C_l cos\phi+C_d sin\phi. \quad (A.\ 23)$$

This provides all the terms required to determine damping derivatives.

Appendix B

For the 9th to 21st modes, the eigenfrequencies, damping ratios are listed in Table B.1.

Table B.1. Eigenfrequencies and damping factors the 9th to 21st modes; turbine in operation; mean wind speed 20 m/s.

Mode Number	Frequency (Hz)	Damping Ratio (%)	Mode Number	Frequency (Hz)	Damping Ratio (%)
9	1.63	18.7	16	4.02	5.2
10	1.98	15.4	17	4.17	2.7
11	2.03	15.0	18	4.52	8.5
12	2.97	6.9	19	4.56	8.6
13	3.11	9.1	20	7.08	10.1
14	3.76	2.8	21	7.84	9.7
15	3.99	9.9			